Parametric Near-field-to-far-field Transformation by Precomputed Empirical-interpolation Patches

A. Sommer, O. Floch, O. Farle, and R. Dyczij-Edlinger
Chair for Electromagnetic Theory, Saarland University, Saarbrücken D-66123, Germany

Abstract— This paper presents an efficient parametric near-field-to-far-field transformation technique for electrically large antenna arrays. The suggested approach combines a sub-domain strategy on the Huygens surface with precomputed empirical-interpolation patches. A real-world example is provided to demonstrate the efficiency and accuracy of the proposed method.

1. INTRODUCTION

Using conventional finite-element (FE) methods, the broadband analysis of antenna arrays and the resulting far-fields tends to be computationally demanding, because the FE systems are of large size and need to be solved at a high number of frequency points. Methods of order-reduction provide an attractive alternative. They need some extra time to construct a reduced-order model (ROM), but the ROM itself is so cheap to solve that evaluation time is usually dominated by the costs of the near-field-to-far-field (NF-FF) transformation. To improve runtimes even further, it was suggested in [1, 2] to replace the steps of field reconstruction on the Huygens surface and subsequent NF-FF transformation by a procedure that computes the far-fields directly from the ROM. For this purpose, an affine approximation to the NF-FF operator is constructed by the empirical interpolation method (EIM) [3]. The suggested approach greatly accelerates the *online* computation of far-fields, at the price of increased *offline* time for constructing the model.

In a previous paper [4], the authors proposed a sub-domain approach on the Huygens surface that allows to restrict the EIM domain to a small number of reference surfaces. Since the sub-face areas are much smaller than that of the entire Huygens surface, the offline part of the EIM is performed much more efficiently. Still, the EIM offline step is not cheap and needs to be done for every antenna structure anew. The present work shows that the offline part of the EIM may be computed upfront, without reference to a specific FE model. The resulting data structures are stored as templates which may be incorporated into ROMs later on, by cheap scaling and compression steps. The proposed method computes an affine approximation to the NF-FF operator for the Huygens surface similarly to [4] and supports fast online computation of far-fields as a function of frequency and observation angles. Section 5 presents a real-world example that demonstrates the efficiency and accuracy of the suggested approach.

2. FAR-FIELD COMPUTATION

2.1. Vector Huygens Principle

By the vector Huygens principle in the frequency domain [5], the radiation vector $\boldsymbol{F}$ of an arbitrary antenna array enclosed by a surface S is given by

$$\boldsymbol{F}\left(k_0, \hat{\boldsymbol{r}}\right) = \hat{\boldsymbol{r}} \times \oint_S e^{jk_0 \hat{\boldsymbol{r}}\cdot\boldsymbol{r}'} \boldsymbol{J}_s\left(\boldsymbol{r}', k_0\right) \, \mathrm{d}S' \times \hat{\boldsymbol{r}} + \frac{1}{\eta_0} \oint_S e^{jk_0 \hat{\boldsymbol{r}}\cdot\boldsymbol{r}'} \boldsymbol{M}_s\left(\boldsymbol{r}', k_0\right) \, \mathrm{d}S' \times \hat{\boldsymbol{r}}. \tag{1}$$

Here η_0 denotes the characteristic impedance of vacuum, the unit vector $\hat{\boldsymbol{r}}$ represents the direction to the observer, and k_0 stands for the vacuum wavenumber, which is related to the vacuum wavelength λ_0 by $k_0 = \frac{2\pi}{\lambda_0}$. The equivalent electric and magnetic surface current densities, $\boldsymbol{J}_s$ and $\boldsymbol{M}_s$, are given in terms of the electric and magnetic near-fields $\boldsymbol{E}$ and $\boldsymbol{H}$ by

$$\boldsymbol{J}_s\left(\boldsymbol{r}', k_0\right) = \hat{\boldsymbol{n}} \times \boldsymbol{H}\left(\boldsymbol{r}', k_0\right) \quad \text{and} \quad \boldsymbol{M}_s\left(\boldsymbol{r}', k_0\right) = -\hat{\boldsymbol{n}} \times \boldsymbol{E}\left(\boldsymbol{r}', k_0\right) \quad \text{with} \quad \boldsymbol{r}' \in S. \tag{2}$$

Herein, $\hat{\boldsymbol{n}}$ denotes the outward-pointing unit normal vector on the Huygens surface S. The far-fields $\boldsymbol{E}_F$ and $\boldsymbol{H}_F$ are determined from (1) by

$$\boldsymbol{E}_F\left(k_0, \boldsymbol{r}\right) = -j\eta_0 k_0 \frac{e^{-jk_0 r}}{4\pi r} \boldsymbol{F}\left(k_0, \hat{\boldsymbol{r}}\right) \quad \text{and} \quad \boldsymbol{H}_F\left(k_0, \boldsymbol{r}\right) = -jk_0 \frac{e^{-jk_0 r}}{4\pi r} \hat{\boldsymbol{r}} \times \boldsymbol{F}\left(k_0, \hat{\boldsymbol{r}}\right). \tag{3}$$

2.2. Numerical Near-Field Computation

FE discretization of an array of T antennas results in a linear system of the form

$$\left(\mathbf{A}_0 + k_0\mathbf{A}_1 + k_0^2\,\mathbf{A}_2\right)\mathbf{x}\left(k_0\right) = k_0\sum_{p=1}^{T}\mathbf{b}_p, \tag{4a}$$

$$\mathbf{y}_0\left(k_0\right) = k_0^{-1}\mathbf{C}\,\mathbf{x}\left(k_0\right), \tag{4b}$$

$$\mathbf{y}_1\left(k_0\right) = \mathbf{D}\,\mathbf{x}\left(k_0\right), \tag{4c}$$

where $\mathbf{A}_0, \mathbf{A}_1, \mathbf{A}_2 \in \mathbb{C}^{N\times N}$ denote the stiffness, damping, and mass matrices, respectively, $\mathbf{x}$ is the solution vector in terms of $\boldsymbol{E}$, and N the dimension of the FE system. The output vectors $\mathbf{y}_0 \in \mathbb{C}^{3H}$ and $\mathbf{y}_1 \in \mathbb{C}^{3H}$ hold the values of the equivalent electric and magnetic surface current densities $\boldsymbol{J}_s$ and $\boldsymbol{M}_s$, respectively, sampled at H points on the Huygens surface S. The matrices $\mathbf{C} \in \mathbb{C}^{3H\times N}$ and $\mathbf{D} \in \mathbb{C}^{3H\times N}$ carry out the sampling process. The RHS of (4a) is constructed by a superposition of T linearly independent vectors $\mathbf{b}_p \in \mathbb{C}^N$.

2.3. Numerical Near-Field-to-Far-Field Transformation

Once the equivalent surface current densities on the Huygens surface S have been computed, a post-processing step is necessary to determine the far-fields of the antenna array. Without loss of generality, we just consider the x component of the second integral in (1). Applying a midpoint quadrature rule with H patches of area ΔS_h leads to

$$I_x\left(k_0, \hat{\boldsymbol{r}}\right) = \oint_S e\left(\boldsymbol{r}', k_0, \hat{\boldsymbol{r}}\right) M_{s,x}\left(\boldsymbol{r}', k_0\right)\,\mathrm{d}S' \approx \sum_{h=1}^{H} e\left(\boldsymbol{r}'_h, k_0, \hat{\boldsymbol{r}}\right) M_{s,x}\left(\boldsymbol{r}'_h, k_0\right)\Delta S'_h \tag{5}$$

with

$$e\left(\boldsymbol{r}', k_0, \hat{\boldsymbol{r}}\right) = e^{jk_0\hat{\boldsymbol{r}}\cdot\boldsymbol{r}'}. \tag{6}$$

We express the direction $\hat{\boldsymbol{r}}$ in terms of the look angles (θ, ϕ) and introduce the parameter vector $\mathbf{p} = (k_0, \theta, \phi) \in \mathcal{D} \subset \mathbb{R}^3$, where $\mathcal{D}$ stands for the considered parameter domain. Given a sampling point $\boldsymbol{r}'_h \in S$, we denote by $\mathbf{D}(\boldsymbol{r}'_h) \in \mathbb{C}^{3\times N}$ the corresponding rows of $\mathbf{D}$. By expressing the surface current densities $\boldsymbol{M}(\boldsymbol{r}'_h)$ by means of the FE solution $\mathbf{x}(k_0)$ according to (4c) we arrive at

$$I_x\left(\mathbf{p}\right) = \sum_{h=1}^{H} e\left(\boldsymbol{r}'_h, \mathbf{p}\right)\,\mathbf{Q}\left(\boldsymbol{r}'_h\right)\,\mathbf{x}\left(k_0\right) \qquad \text{with} \quad \mathbf{Q}\left(\boldsymbol{r}'_h\right) = \Delta S'_h\,\mathbf{D}_x\left(\boldsymbol{r}'_h\right),\ \mathbf{Q} \in \mathbb{C}^{H\times N}. \tag{7}$$

3. FAR-FIELD COMPUTATION BY ORDER REDUCTION

3.1. Near-Field Computation by Model Order Reduction

To obtain the equivalent electric and magnetic surface current densities, the large-scale system (4) has to be solved at each operating point k_0 of interest. Our aim now is to bypass this time-consuming procedure by employing a model order reduction (MOR) method: We denote the wavenumber interval under consideration by $\mathcal{D}_k \subset \mathbb{R}$, such that $k_0 \in \mathcal{D}_k$. Thanks to affine parameter-dependence [6] on k_0, the underlying FE model is well-suited for projection-based MOR. The idea of this method is to approximate the FE solution $\mathbf{x}\left(k_0\right)$ in a low-dimensional subspace according to

$$\mathbf{x}\left(k_0\right) \approx \hat{\mathbf{x}}\left(k_0\right) = \mathbf{V}\tilde{\mathbf{x}}\left(k_0\right) \qquad \forall k_0 \in \mathcal{D}_k \tag{8}$$

with $\hat{\mathbf{x}} \in \mathbb{C}^N, \tilde{\mathbf{x}} \in \mathbb{C}^n, \mathbf{V} \in \mathbb{C}^{N\times n}$ and $n \ll N$. For numerical robustness, the columns of the trial matrix $\mathbf{V}$ are chosen to be orthogonal. Substituting the approximation (8) for the FE solution $\mathbf{x}\left(k_0\right)$ in (4a) and subsequent testing with $\mathbf{V}^*$ leads to a reduced order model (ROM) of the form

$$\sum_{q=0}^{2} k_0^q\tilde{\mathbf{A}}_q\tilde{\mathbf{x}}\left(k_0\right) = k_0\sum_{i=1}^{T}\tilde{\mathbf{b}}_i, \tag{9a}$$

$$\hat{\mathbf{y}}_0\left(k_0\right) = \tilde{\mathbf{C}}\,\tilde{\mathbf{x}}\left(k_0\right), \tag{9b}$$

$$\hat{\mathbf{y}}_1\left(k_0\right) = k_0^{-1}\tilde{\mathbf{D}}\,\tilde{\mathbf{x}}\left(k_0\right), \tag{9c}$$

wherein the reduced matrices and vectors are given by

$$\tilde{\mathbf{A}}_q = \mathbf{V}^* \mathbf{A}_q \mathbf{V} \quad \text{with} \quad \tilde{\mathbf{A}}_q \in \mathbb{C}^{n \times n}, \tag{10a}$$
$$\tilde{\mathbf{b}}_i = \mathbf{V}^* \mathbf{b}_i \quad \text{with} \quad \tilde{\mathbf{b}}_i \in \mathbb{C}^{n}, \tag{10b}$$
$$\tilde{\mathbf{C}} = \mathbf{C}\mathbf{V} \quad \text{with} \quad \tilde{\mathbf{C}} \in \mathbb{C}^{3H \times n}, \tag{10c}$$
$$\tilde{\mathbf{D}} = \mathbf{D}\mathbf{V} \quad \text{with} \quad \tilde{\mathbf{D}} \in \mathbb{C}^{3H \times n}. \tag{10d}$$

Using a multi-point (MP) MOR method, the trial matrix $\mathbf{V}$ is constructed from the FE solutions on a discrete set $\mathcal{D}_{k,e} \subset \mathcal{D}_k$ of expansion points $k_{0,i} \in \mathcal{D}_{k,e}$ such that

$$\text{range}\mathbf{V} = \text{span}\left\{\mathbf{x}\left(k_{0,1}\right), \ldots, \mathbf{x}\left(k_{0,n}\right)\right\}. \tag{11}$$

To obtain appropriate expansion points, we apply a greedy method with self-adaptive expansion point selection [1]. Since, in practice, $n \ll N$, the ROM (9) is solved much more efficiently than the original FE model (4). Hence, the computational efforts for determining the equivalent surface current densities are greatly reduced.

3.2. NF-FF Transformation by Empirical Interpolation

Substituting the ROM approximation (8) for $\mathbf{x}(k_0)$ in (7) leads to

$$I_x\left(\tilde{\mathbf{x}}\left(k_0\right), \mathbf{p}\right) = \sum_{h=1}^{H} e\left(\boldsymbol{r}'_h, \mathbf{p}\right)\, \tilde{\mathbf{Q}}\left(\boldsymbol{r}'_h\right)\, \tilde{\mathbf{x}}\left(k_0\right) \qquad \text{with} \quad \tilde{\mathbf{Q}} = \mathbf{Q}\mathbf{V},\ \tilde{\mathbf{Q}} \in \mathbb{C}^{H \times n}. \tag{12}$$

It can be seen that, even though the solution $\tilde{\mathbf{x}}(k_0)$ of the ROM (9) is used, still $O(H + Hn)$ online operations are required to evaluate (12) for a given parameter point $\mathbf{p} \in \mathcal{D}$. Thus, the complexity of the far-field computation depends on the dimension H of the original FE model (4).

To reduce computational costs, we adopt an approach from [1] and construct an affine approximation to the exponential function (6) by the EIM [3]. In the offline part of this method, a greedy algorithm is applied to determine a set of M basis functions $\{q_m\}_{m=1}^{M}$, interpolation points $\{\boldsymbol{r}'_m\}_{m=1}^{M}$, and parameter values $\{\mathbf{p}_m\}_{m=1}^{M}$ such that the interpolant defined by

$$\hat{e}\left(\boldsymbol{r}', \mathbf{p}\right) = \sum_{m=1}^{M} \alpha_m\left(\mathbf{p}\right) q_m\left(\boldsymbol{r}'\right) \tag{13}$$

approximates (6) for all $(\boldsymbol{r}', \mathbf{p}) \in S \times \mathcal{D}$. The parameter-dependent coefficients $\{\alpha_m\left(\mathbf{p}\right)\}_{m=1}^{M}$ are determined online, by solving the lower triangular system

$$\left[\mathbf{B}_M\right] \begin{bmatrix} \alpha_1\left(\mathbf{p}\right) \\ \vdots \\ \alpha_M\left(\mathbf{p}\right) \end{bmatrix} = \begin{bmatrix} e\left(\boldsymbol{r}'_1, \mathbf{p}\right) \\ \vdots \\ e\left(\boldsymbol{r}'_M, \mathbf{p}\right) \end{bmatrix} \qquad \text{with} \qquad \mathbf{B}_M = \begin{bmatrix} q_1\left(\boldsymbol{r}'_1\right) & & \\ \vdots & \ddots & \\ q_1\left(\boldsymbol{r}'_M\right) & \ldots & q_M\left(\boldsymbol{r}'_M\right) \end{bmatrix}, \tag{14}$$

which is of complexity $O\left(M^2\right)$. Expressing the interpolant (13) by means of ${\mathbf{B}_M}^{-1}$ leads to

$$\hat{e}\left(\boldsymbol{r}', \mathbf{p}\right) = \left[q_1\left(\boldsymbol{r}'\right), \ldots, q_M\left(\boldsymbol{r}'\right)\right]\left[\mathbf{B}_M\right]^{-1}\left[e\left(\boldsymbol{r}'_1, \mathbf{p}\right), \ldots, e\left(\boldsymbol{r}'_M, \mathbf{p}\right)\right]^T = \sum_{m=1}^{M} e\left(\boldsymbol{r}'_m, \mathbf{p}\right) v_m\left(\boldsymbol{r}'\right). \tag{15}$$

Since we wish to compute the expression (6) on a fixed finite set of sampling points $\{\boldsymbol{r}'_h\}_{h=1}^{H}$, the determination of the basis functions $\{v_m\}_{m=1}^{M}$ can be performed offline. Thus, in the online part of the EI method, we just need to evaluate (15), which is of complexity $O\left(M\right)$. Substituting the approximation (15) for $e\left(\boldsymbol{r}', \mathbf{p}\right)$ in (7) results in

$$I_x\left(\tilde{\mathbf{x}}\left(k_0\right), \mathbf{p}\right) = \sum_{m=1}^{M} e\left(\boldsymbol{r}'_m, \mathbf{p}\right) \mathbf{w}_m\, \tilde{\mathbf{x}}\left(k_0\right) \quad \text{with} \quad \mathbf{w}_m = \sum_{h=1}^{H} v_m\left(\boldsymbol{r}'_h\right) \tilde{\mathbf{Q}}\left(\boldsymbol{r}'_h\right), \ \mathbf{w}_m \in \mathbb{C}^{1 \times n}. \tag{16}$$

Hence, the computational costs of the post-processing step, i.e., the evaluation of (16) for a given parameter point $\mathbf{p} \in \mathcal{D}$, are just of order $O\left(M + Mn\right)$. Since in practice we always have $M \ll H$, the far-fields of the antenna array are computed efficiently.

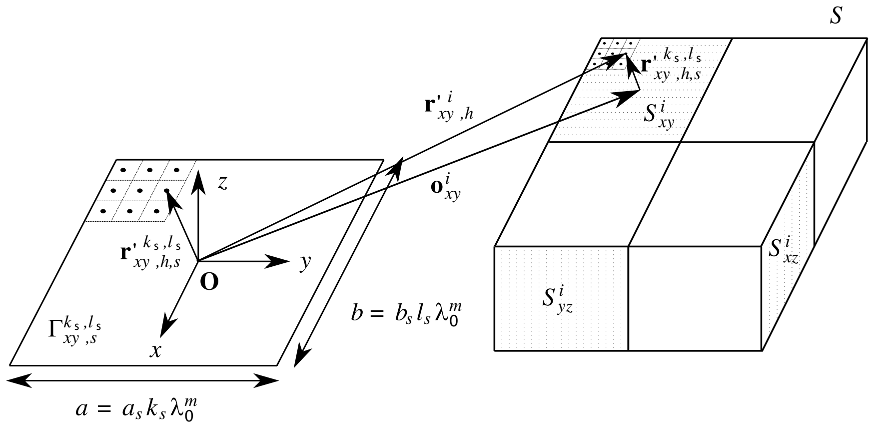

Figure 1: Sub-domain strategy on the Huygens surface S using precomputed EIM patches.

4. NF-FF TRANSFORMATION BY PRECOMPUTED EIM PATCHES

While the online strategy of Section 3.2 for EIM-based far-field computation is of low complexity, the offline part of the method tends to be rather time-consuming, especially when the considered structures become electrically large. As a remedy, we propose to employ precomputed EIM patches rather than to perform the offline part of the EIM for every antenna array anew. For this purpose, the Huygens surface S is taken to be a box, whose surfaces are partitioned into a number of equal sub-faces S^i_{xy}, S^i_{xz} and S^i_{yz}, according to Figure 1:

$$S = \left(\bigcup_{i=1}^{L_{xy}} S^i_{xy}\right) \cup \left(\bigcup_{i=1}^{L_{xz}} S^i_{xz}\right) \cup \left(\bigcup_{i=1}^{L_{yz}} S^i_{yz}\right). \tag{17}$$

Without loss of generality, we consider the sub-faces $\{S^i_{xy}\}_{i=1}^{L_{xy}}$ in the xy plane.

4.1. Computation of EIM Patches

We introduce the parameter vector $\mathbf{d} = (\theta, \phi) \in \mathcal{B}$, where $\mathcal{B} = [0, \pi] \times [0, 2\pi)\,\mathrm{rad}^2 \subset \mathbb{R}^2$ denotes the domain of all possible look angles (θ, ϕ), and the normalized vector $\boldsymbol{r}'_\lambda$, defined by $\boldsymbol{r}'_\lambda = \frac{1}{\lambda_0}\boldsymbol{r}'$. With the help of $\boldsymbol{r}'_\lambda$ and $\mathbf{d}$, the exponential function (6) is rewritten as

$$e\left(\boldsymbol{r}'_\lambda, \mathbf{d}\right) = e^{j2\pi\hat{\boldsymbol{r}}(\mathbf{d})\cdot\boldsymbol{r}'_\lambda}. \tag{18}$$

Next, we define two sets of K^2 reference sub-faces $\{\{\Gamma^{k,l}_{xy}\}_{k=1}^K\}_{l=1}^K$ and $\{\{\Gamma^{k,l,\lambda}_{xy}\}_{k=1}^K\}_{l=1}^K$ by

$$\Gamma^{k,l}_{xy} := \left\{(x,y,z) \in \mathbb{R}^3 \;\middle|\; -k\frac{\lambda_0}{2} \le x \le k\frac{\lambda_0}{2}, \quad -l\frac{\lambda_0}{2} \le y \le l\frac{\lambda_0}{2}, \quad z = 0\right\}, \tag{19}$$

$$\Gamma^{k,l,\lambda}_{xy} := \left\{(x,y,z) \in \mathbb{R}^3 \;\middle|\; -\frac{k}{2} \le x \le \frac{k}{2}, \quad -\frac{l}{2} \le y \le \frac{l}{2}, \quad z = 0\right\}. \tag{20}$$

Then, we construct the empirical interpolants $\{\{\hat{e}^{k,l}_{xy}\}_{k=1}^K\}_{l=1}^K$ of the exponential function (18) for all $(\mathbf{r}'_\lambda, \mathbf{d}) \in \Gamma^{k,l,\lambda}_{xy} \times \mathcal{B}$ according to

$$\hat{e}^{k,l}_{xy}\left(\boldsymbol{r}'_\lambda, \mathbf{d}\right) = \sum_{m=1}^{M^{k,l}_{xy}} e\left(\boldsymbol{r}'^{\,k,l,\lambda}_{xy,m}, \mathbf{d}\right) v^{k,l}_{xy,m}\left(\boldsymbol{r}'_\lambda\right). \tag{21}$$

Finally, we determine for each $(k,l) \in \{1, \cdots, K\} \times \{1, \cdots, K\}$ two sets of equidistantly sampled points $\Gamma^{k,l}_{d,xy} \subset \Gamma^{k,l}_{xy}$ and $\Gamma^{k,l,\lambda}_{d,xy} \subset \Gamma^{k,l,\lambda}_{xy}$ using an appropriate sampling rate r_s,

$$\Gamma^{k,l}_{d,xy} = \left\{\boldsymbol{r}'^{\,k,l}_{xy,h}\right\}_{h=1}^{H^{k,l}_{xy}} \quad \text{and} \quad \Gamma^{k,l,\lambda}_{d,xy} = \left\{\boldsymbol{r}'^{\,k,l,\lambda}_{xy,h}\right\}_{h=1}^{H^{k,l}_{xy}} \quad \text{with} \quad H^{k,l}_{xy} = kl\left(r_s\right)^2, \tag{22}$$

and compute the basis functions $\left\{v^{k,l}_{xy,m}\right\}_{m=1}^{M^{k,l}_{xy}}$ for all $\boldsymbol{r}'_\lambda \in \Gamma^{k,l,\lambda}_{d,xy}$ offline.

4.2. Application of Precomputed EIM Patches

Let $a \times b$ be the size of the sub-faces $\{S_{xy}^i\}_{i=1}^{L_{xy}}$, and let the following condition hold for the maximum wavenumber $k_0^m \in \mathcal{D}_k$ and the corresponding wavelength λ_0^m:

$$\max\{a, b\} \leq K\lambda_0^m. \tag{23}$$

We select the reference sub-face $\Gamma_{xy}^{k_s,l_s} \in \{\{\Gamma_{xy}^{k,l}\}_{k=1}^K\}_{l=1}^K$ according to

$$k_s = \left\{k \in \{1, \cdots, K\} \;\middle|\; \min_k (a \leq k\lambda_0^m)\right\} \quad \text{and} \quad l_s = \left\{l \in \{1, \cdots, K\} \;\middle|\; \min_l (b \leq l\lambda_0^m)\right\} \tag{24}$$

and determine the scaling factors $a_s = \frac{a}{k_s\lambda_0^m}$ and $b_s = \frac{b}{l_s\lambda_0^m}$. Furthermore, we scale the x and y dimension of the reference sub-face $\Gamma_{xy}^{k_s,l_s}(\lambda_0^m)$ such that

$$\Gamma_{xy,s}^{k_s,l_s} = \left\{(x, y, z) \in \mathbb{R}^3 \middle| -a_s k_s \frac{\lambda_0^m}{2} \leq x \leq a_s k_s \frac{\lambda_0^m}{2}, -b_s l_s \frac{\lambda_0^m}{2} \leq y \leq b_s l_s \frac{\lambda_0^m}{2}, z = 0\right\} \tag{25}$$

fits in the sub-faces $\{S_{xy}^i\}_{i=1}^{L_{xy}}$. Similarly, we determine the scaled sampling points $\Gamma_{d,xy,s}^{k_s,l_s} = \left\{\boldsymbol{r'}_{xy,h,s}^{k_s,l_s}\right\}_{h=1}^{H_{xy}^{k_s,l_s}}$ and interpolation points $\left\{\boldsymbol{r'}_{xy,m,s}^{k_s,l_s}\right\}_{m=1}^{M_{xy}^{k_s,l_s}}$ by

$$\boldsymbol{r'}_{xy,h,s}^{k_s,l_s} = \operatorname{diag}(a_s, b_s, 1)\, \lambda_0^m \boldsymbol{r'}_{xy,h}^{k_s,l_s,\lambda} \qquad \text{and} \qquad \boldsymbol{r'}_{xy,m,s}^{k_s,l_s} = \operatorname{diag}(a_s, b_s, 1)\, \lambda_0^m \boldsymbol{r'}_{xy,m}^{k_s,l_s,\lambda}. \tag{26}$$

Given a point $\boldsymbol{r'}_{xy,s}^{k_s,l_s}$ on the reference sub-face $\Gamma_{xy,s}^{k_s,l_s}$, the corresponding sampling point $\boldsymbol{r'}_{xy}^i \in S_{xy}^i$ is obtained by adding a constant translation vector $\boldsymbol{o}_{xy}^i$ according to Figure 1: $\boldsymbol{r'}_{xy}^i = \boldsymbol{o}_{xy}^i + \boldsymbol{r'}_{xy,s}^{k_s,l_s}$. Hence, the exponential function (6) is represented as

$$e\left(\boldsymbol{r'}_{xy}^i, \mathbf{p}\right) = e\left(\boldsymbol{o}_{xy}^i, \mathbf{p}\right) e\left(\boldsymbol{r'}_{xy,s}^{k_s,l_s}, \mathbf{p}\right). \tag{27}$$

Proposition 1. *The empirical interpolant* $\hat{e}_{xy}^{k_s,l_s}\left(\boldsymbol{r'}_{xy,s}^{k_s,l_s}, \mathbf{p}\right)$ *defined by*

$$\hat{e}_{xy}^{k_s,l_s}\left(\boldsymbol{r'}_{xy,s}^{k_s,l_s}, \mathbf{p}\right) = \sum_{m=1}^{M_{xy}^{k_s,l_s}} e\left(\boldsymbol{r'}_{xy,m,s}^{k_s,l_s}, \mathbf{p}\right) v_{xy,m}^{k_s,l_s}\left(\boldsymbol{r'}_{xy}^{k_s,l_s,\lambda}\right) \tag{28}$$

with $\boldsymbol{r'}_{xy,s}^{k_s,l_s} = \operatorname{diag}(a_s, b_s, 1)\, \lambda_0^m \boldsymbol{r'}_{xy}^{k_s,l_s,\lambda}$ *approximates* (6) *for all* $\left(\boldsymbol{r'}_{xy,s}^{k_s,l_s}, \mathbf{p}\right) \in \Gamma_{xy,s}^{k_s,l_s} \times \mathcal{D}$.

Proof. Using the basis functions $\left\{v_{xy,m}^{k_s,l_s}\right\}_{m=1}^{M_{xy}^{k_s,l_s}}$ and the interpolation points $\left\{\boldsymbol{r'}_{xy,m}^{k_s,l_s,\lambda}\right\}_{m=1}^{M_{xy}^{k_s,l_s}}$ of Section 4.1, the exponential function (18) is approximated by

$$\hat{e}_{xy}^{k_s,l_s}\left(\boldsymbol{r'}_\lambda, \mathbf{d}\right) = \sum_{m=1}^{M_{xy}^{k_s,l_s}} e\left(\boldsymbol{r'}_{xy,m}^{k_s,l_s,\lambda}, \mathbf{d}\right) v_{xy,m}^{k_s,l_s}\left(\boldsymbol{r'}_\lambda\right) \tag{29}$$

for all $(\boldsymbol{r'}_\lambda, \mathbf{d}) \in \Gamma_{xy}^{k_s,l_s,\lambda} \times \mathcal{B}$. The representation

$$e^{j2\pi\hat{\boldsymbol{r}}(\mathbf{d})\cdot\boldsymbol{r'}_\lambda} = e^{j2\pi\hat{\boldsymbol{r}}(\mathbf{d})\cdot\frac{\lambda_0^m}{\lambda_0^m}\boldsymbol{r'}_\lambda} = e^{j\frac{2\pi}{\lambda_0^m}\hat{\boldsymbol{r}}(\mathbf{d})\cdot\lambda_0^m\boldsymbol{r'}_\lambda} = e^{jk_0^m\hat{\boldsymbol{r}}(\mathbf{d})\cdot\boldsymbol{r'}} \tag{30}$$

shows that the empirical interpolant $\hat{e}_{xy}^{k_s,l_s}$ also approximates the exponential function (6) for all $(\mathbf{r'}, \mathbf{p}) \in \Gamma_{xy}^{k_s,l_s}(\lambda_0^m) \times (\{k_0^m\} \times \mathcal{B})$:

$$\hat{e}_{xy}^{k_s,l_s}\left(\boldsymbol{r'}, \mathbf{p}\right) = \sum_{m=1}^{M_{xy}^{k_s,l_s}} e\left(\boldsymbol{r'}_{xy,m}^{k_s,l_s}, \mathbf{p}\right) v_{xy,m}^{k_s,l_s}\left(\boldsymbol{r'}_\lambda\right) \quad \text{with} \quad \boldsymbol{r'}_{xy,m}^{k_s,l_s} = \lambda_0^m \boldsymbol{r'}_{xy,m}^{k_s,l_s,\lambda}, \quad \boldsymbol{r'} = \lambda_0^m \boldsymbol{r'}_\lambda. \tag{31}$$

Using the representations

$$\begin{aligned} \boldsymbol{r}' &= [x, y, z], && (32)\\ \hat{\boldsymbol{r}} &= [\sin(\theta)\cos(\phi), \sin(\theta)\sin(\phi), \cos(\theta)], && (33)\\ a_x &= k_0^m \sin(\theta)\cos(\phi), && (34)\\ a_y &= k_0^m \sin(\theta)\sin(\phi), && (35)\\ a_z &= k_0^m \cos(\theta), && (36) \end{aligned}$$

the exponential function (30) is rewritten as

$$e^{jk_0^m \hat{\boldsymbol{r}}(\mathbf{d})\cdot\boldsymbol{r}'} = e^{j(k_0^m \sin(\theta)\cos(\phi)x + k_0^m \sin(\theta)\sin(\phi)y + k_0^m \cos(\theta)z)} = e^{j(a_x x + a_y y + a_z z)}. \tag{37}$$

Furthermore, we exploit the fact that the reference sub-face $\Gamma_{xy}^{k_s,l_s}(\lambda_0^m)$ is located in the xy plane: Substituting $\boldsymbol{r}' = (x, y, 0)$ in (37) results in

$$e^{jk_0^m \hat{\boldsymbol{r}}(\mathbf{d})\cdot\boldsymbol{r}'} = e^{j(k_0^m \sin(\theta)\cos(\phi)x + k_0^m \sin(\theta)\sin(\phi)y)} = e^{j(a_x x + a_y y)}. \tag{38}$$

By introducing the parameter domain $\mathcal{M}_{xy}$ defined by

$$\mathcal{M}_{xy} = \left\{(a_x, a_y, a_z) \in \mathbb{R}^3 \;\middle|\; \sqrt{a_x^2 + a_y^2} \le k_0^m, \quad a_z = 0\right\} \tag{39}$$

and the vector $\mathbf{a}_{xy} = (a_x, a_y, 0) \in \mathcal{M}_{xy}$, we obtain the EIM approximation to (38):

$$\hat{e}_{xy}^{k_s,l_s}\left(\boldsymbol{r}', \mathbf{a}_{xy}\right) = \sum_{m=1}^{M_{xy}^{k_s,l_s}} e\left(\boldsymbol{r}'^{k_s,l_s}_{xy,m}, \mathbf{a}_{xy}\right) v_{xy,m}^{k_s,l_s}\left(\boldsymbol{r}'_\lambda\right) \qquad \forall\left(\boldsymbol{r}', \mathbf{a}_{xy}\right) \in \Gamma_{xy}^{k_s,l_s}(\lambda_0^m) \times \mathcal{M}_{xy}. \tag{40}$$

Finally, we consider (6) for an arbitrary $\mathbf{p} = (k_0, \theta, \phi) \in \mathcal{D}$ with $k_0 = s_k k_0^m$ and $s_k \in [0, 1]$, and the scaled vector $\boldsymbol{r}'_s = \mathrm{diag}(a_s, b_s, 1)\,\boldsymbol{r}' \in \Gamma_{xy,s}^{k_s,l_s}$ with $a_s \in [0, 1]$ and $b_s \in [0, 1]$:

$$e^{jk_0 \hat{\boldsymbol{r}}(\mathbf{d})\cdot\boldsymbol{r}'_s} = e^{js_k k_0^m \hat{\boldsymbol{r}}(\mathbf{d})\cdot \mathrm{diag}(a_s,b_s,1)\boldsymbol{r}'} = e^{j(s_k a_s a_x x + s_k b_s a_y y)} = e^{js_k \mathrm{diag}(a_s,b_s,1)\mathbf{a}_{xy}\cdot\boldsymbol{r}'}. \tag{41}$$

Since $s_k\mathrm{diag}(a_s, b_s, 1)\,\mathbf{a}_{xy}$ is included in $\mathcal{M}_{xy}$ and $e(\boldsymbol{r}'_s, \mathbf{p}) = e(\boldsymbol{r}', s_k\mathrm{diag}(a_s, b_s, 1)\,\mathbf{a}_{xy})$, we arrive at the EIM approximation (28):

$$\hat{e}_{xy}^{k_s,l_s}\left(\boldsymbol{r}'_s, \mathbf{p}\right) = \sum_{m=1}^{M_{xy}^{k_s,l_s}} e\left(\boldsymbol{r}'^{k_s,l_s}_{xy,m,s}, \mathbf{p}\right) v_{xy,m}^{k_s,l_s}\left(\boldsymbol{r}'_\lambda\right) \quad \forall\left(\boldsymbol{r}'_s, \mathbf{p}\right) \in \Gamma_{xy,s}^{k_s,l_s} \times \mathcal{D} \tag{42}$$

with $\boldsymbol{r}'_s = \mathrm{diag}(a_s, b_s, 1)\,\lambda_0^m \boldsymbol{r}'_\lambda$ and $\boldsymbol{r}'^{k_s,l_s}_{xy,m,s} = \mathrm{diag}(a_s, b_s, 1)\,\lambda_0^m \boldsymbol{r}'^{k_s,l_s,\lambda}_{xy,m}$. □

Thus it is permissible to use the precomputed basis functions of Section 4.1 and the scaled interpolation points $\left\{\boldsymbol{r}'^{k_s,l_s}_{xy,m,s}\right\}_{m=1}^{M_{xy}^{k_s,l_s}}$ to approximate $e\left(\boldsymbol{r}'^{k_s,l_s}_{xy,h,s}, \mathbf{p}\right)$ for all $\left(\boldsymbol{r}'^{k_s,l_s}_{xy,h,s}, \mathbf{p}\right) \in \Gamma_{d,xy,s}^{k_s,l_s} \times \mathcal{D}$:

$$\hat{e}_{xy}^{k_s,l_s}\left(\boldsymbol{r}'^{k_s,l_s}_{xy,h,s}, \mathbf{p}\right) = \sum_{m=1}^{M_{xy}^{k_s,l_s}} e\left(\boldsymbol{r}'^{k_s,l_s}_{xy,m,s}, \mathbf{p}\right) v_{xy,m}^{k_s,l_s}\left(\boldsymbol{r}'^{k_s,l_s,\lambda}_{xy,h}\right). \tag{43}$$

Substituting (43) in (27), we arrive at the final approximation $\hat{e}_{xy}^i$,

$$\hat{e}_{xy}^i\left(\boldsymbol{r}'^i_{xy,h}, \mathbf{p}\right) = e\left(\boldsymbol{o}_{xy}^i, \mathbf{p}\right) \sum_{m=1}^{M_{xy}^{k_s,l_s}} e\left(\boldsymbol{r}'^{k_s,l_s}_{xy,m,s}, \mathbf{p}\right) v_{xy,m}^{k_s,l_s}\left(\boldsymbol{r}'^{k_s,l_s,\lambda}_{xy,h}\right) \quad \forall\left(\boldsymbol{r}'^i_{xy,h}, \mathbf{p}\right) \in S_{d,xy}^i \times \mathcal{D}, \tag{44}$$

where the set $S_{d,xy}^i = \left\{\boldsymbol{r}'^i_{xy,h}\right\}_{h=1}^{H_{xy}^{k_s,l_s}}$ contains the sampling points on the sub-face S_{xy}^i, which are related to $\boldsymbol{r}'^{k_s,l_s}_{xy,h,s}$ by $\boldsymbol{r}'^i_{xy,h} = \boldsymbol{o}_{xy}^i + \boldsymbol{r}'^{k_s,l_s}_{xy,h,s}$.

Table 1: Computational data for radiation pattern at $f = 10.3\,\mathrm{GHz}$.

General parameters	Frequency range	$[9, 11]\,\mathrm{GHz}$
	Dimension of Huygens box $a_S \times b_S \times c_S$	$0.2 \times 0.0316 \times 0.2\,\mathrm{m}^3$
	Number of look angles P	57,121
	Sampling rate r_s (per λ_0^m)	20
Conventional method	FE dimension N	2,088,966
	Number of sampling points H	57,330
	Time[1,2] for solving FE system (4a)	58.14 s
	Time[1] for NF-FF transformation for a given $\mathbf{p} \in \mathcal{D}$	$3.062 \cdot 10^{-2}$ s
Proposed method	ROM dimension n	9
	Number of precomputed EIM-patches K^2	100
	Number of sub-faces L_{xy}, L_{xz}, L_{yz}	4, 2, 4
	Selected reference sub-faces $\Gamma_{xy}^{k_s,l_s}$, $\Gamma_{xz}^{k_s,l_s}$, $\Gamma_{yz}^{k_s,l_s}$	$\Gamma_{xy}^{8,1}$, $\Gamma_{xz}^{8,8}$, $\Gamma_{yz}^{1,8}$
	Scaling factors (a_s, b_s) for xy plane	$(0.9173, 0.5794)$
	Scaling factors (a_s, c_s) for xz plane	$(0.9173, 0.9173)$
	Scaling factors (b_s, c_s) for yz plane	$(0.5794, 0.9173)$
	Number of EIM interpolation points M_t	2,760
	Time[1] for solving ROM (9a)	$4.566 \cdot 10^{-5}$ s
	Time[1] for NF-FF transformation for a given $\mathbf{p} \in \mathcal{D}$	$1.73 \cdot 10^{-3}$ s
	Average error e_D	$1.306 \cdot 10^{-4}$

[1]MATLAB R2012a on Intel® Core™ i7-2600K CPU @ 3,40 GHz.
[2]Intel® MKL 10.2.1 PARDISO for solving sparse linear systems of equations.

4.3. Far-Field Computation by Precomputed EIM Patches

Using the solution (8) and the sampling points $\left\{S_{d,xy}^i\right\}_{i=1}^{L_{xy}}$ on the sub-faces $\left\{S_{xy}^i\right\}_{i=1}^{L_xy}$, we obtain

$$I_{x,xy}\left(\tilde{\mathbf{x}}\left(k_0\right), \mathbf{p}\right) = \sum_{i=1}^{L_{xy}} \sum_{h=1}^{H_{xy}^{k_s,l_s}} e\left(\boldsymbol{r'}_{xy,h}^{i}, \mathbf{p}\right)\, \tilde{\mathbf{Q}}\left(\boldsymbol{r'}_{xy,h}^{i}\right)\, \tilde{\mathbf{x}}\left(k_0\right). \tag{45}$$

Substituting (44) for $e\left(\boldsymbol{r'}_{xy,h}^{i}, \mathbf{p}\right)$ in (45) leads to the final approximation $\hat{I}_{x,xy}$:

$$\hat{I}_{x,xy}\left(\mathbf{p}\right) = \sum_{i=1}^{L_{xy}} e\left(\boldsymbol{o}_{xy}^i, \mathbf{p}\right) \sum_{m=1}^{M_{xy}^{k_s,l_s}} e\left(\boldsymbol{r'}_{xy,m,s}^{k_s,l_s}, \mathbf{p}\right) \left(\sum_{h=1}^{H_{xy}^{k_s,l_s}} v_{xy,m}^{k_s,l_s}\left(\boldsymbol{r'}_{xy,h}^{k_s,l_s,\lambda}\right) \tilde{\mathbf{Q}}\left(\boldsymbol{r'}_{xy,h}^{i}\right)\right) \tilde{\mathbf{x}}\left(k_0\right). \tag{46}$$

The contributions $\hat{I}_{x,xz}$ and $\hat{I}_{x,yz}$ of the surfaces parallel to the xz and yz planes are obtained in analogous fashion. Hence the approximation $\hat{I}_x$ due to the equivalent surface current densities $M_{s,x}$ on the Huygens surface S is given by

$$\hat{I}_x\left(\mathbf{p}\right) = \hat{I}_{x,xy}\left(\mathbf{p}\right) + \hat{I}_{x,xz}\left(\mathbf{p}\right) + \hat{I}_{x,yz}\left(\mathbf{p}\right). \tag{47}$$

Let $M_t = L_{xy}M_{xy}^{k_s,l_s} + L_{xz}M_{xz}^{k_s,l_s} + L_{yz}M_{yz}^{k_s,l_s}$ denote the total number of EIM interpolation points. Then the online costs for computing the far-field for a given parameter point $\mathbf{p} \in \mathcal{D}$ by (47) are of order $O\left(M_t + M_t n\right)$. If $M_t < H$ holds, which is to be expected in practice, this compares favorably to $O\left(H + Hn\right)$ for the conventional NF-FF transformation.

5. NUMERICAL RESULTS

We consider the FE model of a 10×10 patch antenna array (PAA). The considered frequency band is given by $f \in [9, 11]\,\mathrm{GHz}$, and the look angles of interest are in the range of $(\theta, \phi) \in [0, \pi]\times[0, \pi]\ \mathrm{rad}^2$. We construct the ROM (9) of the PAA for $\mathcal{D}_k$ by the MP-MOR method of Section 3.1. According to Section 4, the Huygens surface S is partitioned into $L = L_{xy} + L_{xz} + L_{yz}$ sub-faces, and appropriate empirical interpolants $\hat{e}_{xy}^{k_s,l_s}, \hat{e}_{xz}^{k_s,l_s}, \hat{e}_{yz}^{k_s,l_s}$ are selected by (24). To investigate the accuracy of the proposed method, we consider the average relative error in directive gain $D(k_0, \theta, \phi)$ [7]:

$$e_D\left(k_0\right) = \frac{1}{P}\sum_{p=1}^{P}\left|\frac{D\left(k_0, \theta_p, \phi_p\right) - \hat{D}\left(k_0, \theta_p, \phi_p\right)}{D\left(k_0, \theta_p, \phi_p\right)}\right|. \tag{48}$$

Herein, P denotes the number of considered look angles (θ_p, ϕ_p). Figure 2 shows the radiation pattern of the 10×10 PAA, determined by the combined use of the ROM (9) and the suggested NF-FF transformation technique of Section 4. Computational data are listed in Table 5. It can be seen that the far-field computation time for a given parameter vector $\mathbf{p} \in \mathcal{D}$ is reduced from 58.17 s to $1.776 \cdot 10^{-3}$, which corresponds to a speed-up factor of more than $3.27 \cdot 10^4$. In addition, the proposed method achieves high accuracy: The average error in directive gain is just $1.306 \cdot 10^{-4}$.

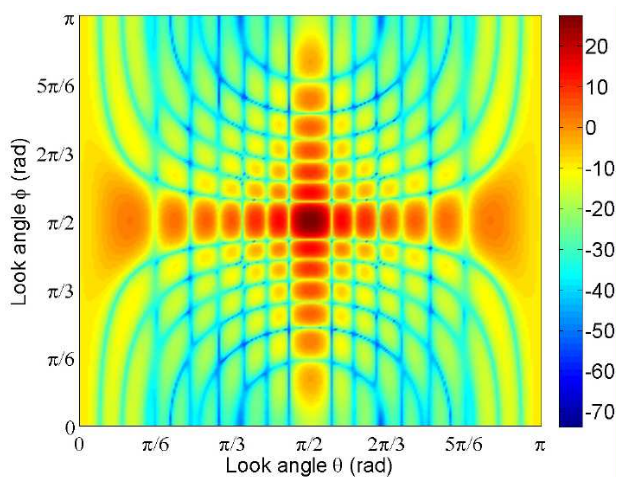

Figure 2: Radiation pattern of the 10×10 PAA at $f = 10.3$ GHz, using $P = 57,121$ look angles.

6. CONCLUSION

The proposed MOR approach provides an efficient and accurate method for computing the far-fields of antenna arrays as a function of frequency and observation direction. Since the NF-FF transformation is based on precomputed EIM patches, it is no longer necessary to perform the time-consuming offline part of the EIM for every antenna array anew. The efficiency and accuracy of the suggested method have been demonstrated by a numerical example.

REFERENCES

1. Fares, M., J. S. Hesthaven, Y. Maday, and B. Stamm, "The reduced basis method for the electric field integral equation," *J. Comput. Phys.* , Vol. 230, No. 14, 5532–5555, 2011.
2. Sommer, A., O. Farle, and R. Dyczij-Edlinger, "Efficient finite-element computation of far-fields of phased arrays by order reduction," *COMPEL* , Vol. 32, No. 5, 1721–1734, 2013.
3. Barrault, M., Y. Maday, N. C. Nguyen, and A. T. Patera, "An 'empirical interpolation' method: Application to efficient reduced-basis discretization of partial differential equations," *C. R. Math. Acad. Sci. Paris* , Vol. 339, No. 9, 1721–1734, 2013.
4. Sommer, A., O. Floch, O. Farle, R. Baltes, and R. Dyczij-Edlinger, "An efficient parametric near-field-to-far-field transformation technique," *Proceedings of the 2013 International Conference on Electromagnetics in Advanced Applications*, 332–335, Torino, Italy, September 2013.
5. Rothwell, E. and M. Cloud, *Electromagnetics*, 2nd Edition, CRC Press, 2008.
6. Rozza, G., D. B. P. Huynh, and A. T. Patera, "Reduced basis approximation and a posteriori error estimation for affinely parametrized elliptic coercive partial differential equations," *Arch. Comput. Methods Eng.*, Vol. 15, No. 3, 229–275, 2008.
7. Orfanidis, S., *Electromagnetic waves and antennas*, www.ece.rutgers.edu/∼orfanidi/ewa.